Microstructure modification and magnetoresistance enhancement by Ag doping in $La_{2/3}Sr_{1/3}MnO_3$ thin films prepared by dual-beam pulsed laser ablation

2001 J. Phys.: Condens. Matter 13 3419

(http://iopscience.iop.org/0953-8984/13/14/315)

INSTITUTE OF PHYSICS PUBLISHING JOURNAL OF PHYSICS: CONDENSED MATTER

J. Phys.: Condens. Matter **13** (2001) 3419–3431 www.iop.org/Journals/cm PII: S0953-8984(01)21605-1

Microstructure modification and magnetoresistance enhancement by Ag doping in $La_{2/3}Sr_{1/3}MnO_3$ thin films prepared by dual-beam pulsed laser ablation

J Li[1,3], Q Huang[1], Z W Li[1], L P You[1,2], S Y Xu[1] and C K Ong[1]

[1] Centre for Superconducting and Magnetic Materials and Department of Physics, National University of Singapore, Lower Kent Ridge Road, Singapore 119260
[2] The Electron Microscopy Laboratory, Peking University, Beijing 100871, People's Republic of China

Received 2 February 2001, in final form 1 March 2001

Abstract

The inter-grain extrinsic magnetoresistance (eMR) observed in polycrystalline perovskite manganites has attracted attention recently. Previous efforts aimed at eMR enhancement have concentrated on grain boundary (GB) modification, mainly by insulator doping. In this paper, however, we report our investigations on the doping effect of a metal, Ag, on the eMR phenomenon. $La_{2/3}Sr_{1/3}MnO_3$ (LSMO) thin films were deposited with varying Ag precipitation on (001) $LaAlO_3$ at different substrate temperatures (T_s) by a dual-beam pulsed-laser ablation system. Various analytical techniques were employed to characterize the films. At $T_s = 750\,^{\circ}C$, the films are perfectly epitaxial with their c-axis perpendicular to the film surface. Ag dopant cannot substitute into the LSMO lattice, thus showing no obvious effect on the magneto-transport properties of the film, though it did impair the film in-plane epitaxy and improve the inter-grain diffusion of the lattice atoms. However, grown at lower $T_s = 400\,^{\circ}C$, the films are granular with c-axis texture. The Ag dopant exists at GBs and helps to increase the local Mn spin disorder at GBs, thus enhancing the eMR value by a factor of two compared with the undoped film. Experiment data also suggest that the transport mechanism underlying the Ag-doping enhanced eMR is spin-dependent scattering.

1. Introduction

In the past few years, interest in the perovskite manganites has been focused on the significant inter-grain magnetoresistance (MR) discovered in polycrystalline samples [1–5]. In particular, bulk polycrystalline samples show substantial MR at temperatures much below the magnetic transition temperature T_c, usually in a field of a few hundred Oersted. Different from the *intrinsic* MR observed near T_c, which is believed to be a consequence of a strong spin–phonon

[3] Author to whom correspondence should be addressed.

0953-8984/01/143419+13$30.00

coupling, the MR found at low temperature is referred as *extrinsic* MR (eMR) [5]. It is believed that the grain boundaries (GBs) and phase interfaces, where the ferromagnetic spin alignment shows disordered status to some extent, serves as strong scattering centres for the highly spin-polarized conducting Mn^{3+} e_g electrons and leads to a high zero-field electrical resistance. Application of a moderate magnetic field can readily align the domains associated with the GBs into parallel configuration and drop the resistivity substantially. The microscopic transport mechanism responsible for the eMR has been modelled as spin-polarized tunnelling (SPT) [2] or spin-dependent scattering (SDS) [3]. Both models give MR proportional to (M/M_s) (M is the magnetization and M_s is the saturation value of M) before the magnetic saturation.

Factors that affect the magnetic spin disorder at GBs or phase interfaces are still under exploration. Previous explorations have been focused on microstructure modification [6–12], such as the grain size refinement [8, 9], manganite/insulator co-sintering [10, 11] and amorphous phase generation [12]. The common feature of these processing procedures is to weaken the ferromagnetic interaction between grains by introducing insulator phase to the GBs. The enhancement of eMR was achieved at the expense of significantly increased resistivity, ρ. For example, an 80% CeO_2 co-sintered sample shows eMR as high as 20% in a field of only 500 Oe at 10 K, but the ρ of the sample is about 10^8 mΩ cm. Such a high ρ is impractical for applications. Actually, the doping of insulator phase should not be an indispensable condition in achieving the magnetic disorders at the phase interfaces. As long as the magnetic exchange is interrupted, any impurity, even a nonmagnetic metal, should be able to decouple the grains and cause Mn spin disorder at the interfaces, subsequently resulting in an enhancement in eMR. Moreover, since the high conducting metal provides an easier pathway for current flow between grains, ρ of a manganite with metal phase at the GBs is expected to be much lower.

On the other hand, previous reports [13, 14] on Ag-doped $YBa_2Cu_3O_{7-\delta}$ (YBCO) epitaxial thin films have revealed that Ag is an ideal doping element, for there is no chemical interaction between Ag and the perovskite structures. Ag cannot substitute into the lattice; on the contrary, it only diffuses to GBs or other defects and exists in the form of a metal. Evidence of the existence of metal Ag has even been found in bulk YBCO co-sintered with Ag_2O [13]. Therefore, in this research, we tried to dope Ag into the $La_{2/3}Sr_{1/3}MnO_3$ (LSMO) thin films, and to investigate its effect on film growth, microstructure, chemical constitution, magnetization and magnetoresistance. The objective of this work was to find out whether or not this Ag doping can decouple the grains and cause Mn spin disorder at the GBs, and enhance the eMR, as an insulator does.

As compared with YBCO, the Ag-doped manganites have been reported on only by a few groups [15, 16]. They focused mainly on the doping effect on the crystal structures. So far, only Tao *et al* [16] have studied the doping effect on the MR behaviour of the $LaMnO_3$ compound. However, they claimed that Ag could incorporate into the lattice and substitute La ions, which is inconsistent with the previous studies. No one has studied the doping effect from the special point of view of the GB modification and the enhancement of eMR. Therefore, the result of this study could be useful to further understand the origin of eMR, and help to verify models of the microscopic transport mechanism across GBs. On the other hand, the metal-doping enhanced eMR, if confirmed, would also help in designing appropriate microstructures for practical applications.

2. Experiment

The ceramic $La_{2/3}Sr_{1/3}MnO_3$ (LSMO) target was sintered by conventional solid-state reaction. Co-deposition of LSMO and Ag on (001)-$LaAlO_3$ (ALO) single-crystal substrates were performed by a dual-beam pulsed laser ablation (PLA) system [17]. The details of the

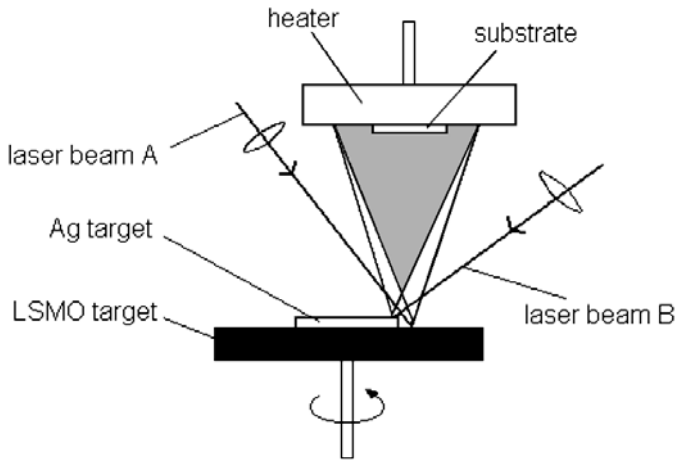

Figure 1. Sketch of the dual-beam pulsed-laser ablation system.

experimental apparatus are illustrated in figure 1. The excimer laser employed was a 248 nm Lambda Physik. Two split laser beams were focused on the coaxial stoichiometric LSMO and metallic Ag targets, respectively, with their spots on the targets close to each other. The substrate was mounted at the cross area of the two plumes. The laser fluency of the two beams was 2.0 J cm^{-2}. While the laser repeat rate for the LSMO was kept at 4 Hz, the repeat rate for the Ag target (Ag repeat rate) could be adjusted from 0 to 8 Hz using a chopper. We deposited films at selected substrate temperatures ranging from 750 to 350 °C, and the films were kept *in situ* for 1 h before cooling down slowly. An oxygen pressure of 0.2 mbar was adopted during the deposition and subsequent annealing procedure. The thicknesses of all the thin films were ∼200 nm. The samples were labelled as *n/4 Ag*, where the *4* and *n* denoted the repeat rate for LSMO and Ag, respectively. For example, *0/4 Ag* denoted a stoichiometric LSMO film; while *8/4 Ag* represented a co-deposited film with Ag repeat rate of 8 Hz.

The film microstructures were determined using fine XRD, atomic force microscopy (AFM) and transmission electron microscopy (TEM). Ag concentration was examined by means of x-ray photoelectron spectroscopy (XPS) and energy dispersive x-ray (EDX). The resistivity and MR was measured using the conventional dc four-probe technique. A triangle wave (0.01 Hz) magnetic field varying from −4 to 4 kOe was applied along the current direction. The cooling and heating rate were well controlled at 1.0 K min^{-1} by a LakeShore 321 autotuning temperature controller. The in-plane magnetization of the sample was obtained using an Oxford vibrating sample magnetometer (VSM).

3. Results

3.1. Film orientation

The fine XRD spectrum of our polycrystalline target is shown in the top panel of figure 2. The bottom panel shows the spectrum of sample *2/4 Ag* deposited at 750 °C as an example of Ag-doped thin films. For consistency, the reflections from the target are also indexed as a pseudo-cubic structure. In the spectrums of all thin films deposited at varying substrate temperature T_s, only (00*l*) peaks of LSMO are observed, besides the reflections contributed by the substrate. There is no peak of Ag or any of the Ag compounds, in spite of the existence of Ag

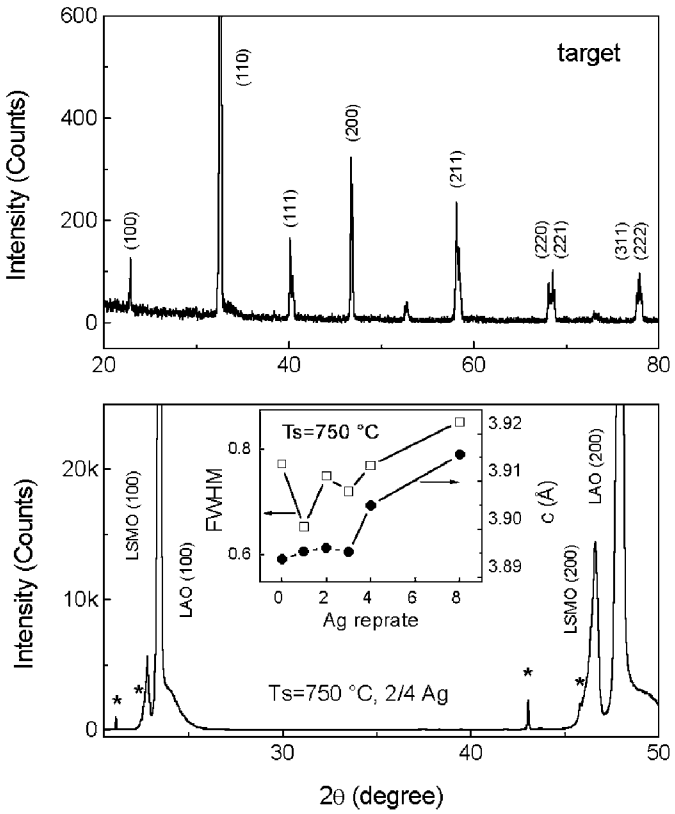

Figure 2. XRD spectrum of the LSMO bulk target and the Ag-doped thin film deposited on (001) LAO at 750 °C. The symbol '*' in the bottom panel denotes reflections from the substrate. The inset shows the FWHM of the (002) LSMO and c parameter for the films deposited with different Ag repeat rates.

precipitation during deposition. With decreasing T_s, and/or with increasing Ag repeat rate, the reflection intensity (normalized by the respective (002) ALO) decreases, implying increased amounts of amorphous phase around GBs. The above-mentioned experimental results reveal the c-axis texture of the films. The Ag dopant, if exists, can only accumulate in the inter-grain amorphous phase. Further investigation also demonstrates the change of lattice parameter along the c axis, c, for the films deposited at the same $T_s = 750\,^{\circ}\mathrm{C}$ but with different Ag repeat rates, as shown in the inset of figure 2. At low and medium doping level, c keeps constant. However, when Ag repeat rate is increased to 4 Hz, c becomes larger. This result suggests the existence of oxygen deficiency in the co-deposited films, which leads to the lattice contraction in the ab plane and expansion along the c-axis [18]. The full width at half maximum (FWHM) of the (002) LSMO is also shown in the same inset. The increase of FWHM at high Ag precipitation is affirmed, which suggests that, in the case of heavy Ag doping, the implanted Ag atoms may help to form some defects in the film.

3.2. Films deposited at $T_s = 750\,^{\circ}C$

Figures 3(a)–(f) show the AFM morphology of the films co-deposited at 750 °C, with Ag repeat rate of 0, 1, 2, 3, 4 and 8 Hz, respectively. The scale for each image is $1 \times 1\ \mu\mathrm{m}^2$. In contrast

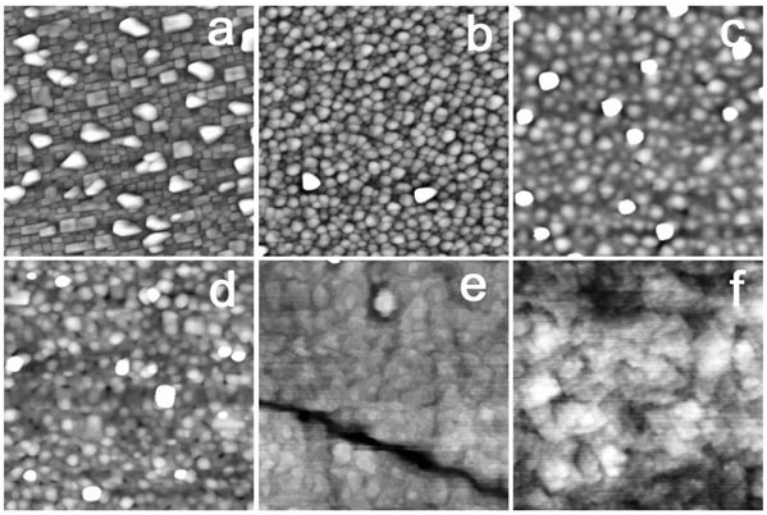

Figure 3. (a)–(f) AFM images for the films co-deposited at 750 °C with Ag repeat rates of 0, 1, 2, 3, 4 and 8 Hz, respectively. The scans areas for the images are all $1 \times 1\ \mu m^2$.

to general observations reported previously, we did not observe any increase in the grain size for the Ag-doped thin films, although it is found that the Ag doping can significantly change the film microstructure. Figure 3(a) is for the stoichiometric LSMO thin film, which consists of rectangular-shaped grains. This mosaic-like grain alignment indicates that the film is not only epitaxial along the *c* axis but also in the *ab* plane, despite the 'droplets' scattering on the surface, which is the characteristic for films deposited by the PLA method. Nevertheless, for the doped film with Ag repeat rate of 1 Hz, the grains are somewhat spherical shaped, as shown in figure 3(b). This suggests deterioration of the in-plane alignment in the Ag co-deposited thin films. At this Ag doping level, however, the GBs are still clear. As the Ag repeat rate increases from 2 to 4 Hz (figures 3(c) and (d)), the grain shape becomes more irregular and the GBs blur gradually. Even the GBs fade when the Ag repeat rate is as high as 8 Hz. These images suggest that the previously observed apparent grain size enlargement due to Ag doping may be attributed to the inter-grain diffusion enhanced by Ag atoms.

Since the XRD results shows no reflection of Ag or any of the Ag compounds, to confirm whether or not Ag exists in the co-deposited films, XPS was employed. Figure 4 records the XPS spectrums for films deposited at 750 °C, with Ag repeat rate varying from 0 to 8 Hz. The intensities of the curves are adjusted on purpose, and the binding energy is calibrated by setting the C 1s line at 285 eV. The curve clearly gives the characteristic spectrum lines of La, Sr, Mn and O elements. If there exists Ag or Ag compounds in the co-deposited films, no matter whether crystal or amorphous, the line corresponding to Ag 3d should be at about 370 eV, as indicated in the figure by symbol '*'. However, no trace of the spectrum line is observed in the energy range from 360 eV to 380 eV, which means that there is no Ag existing at the surface of the films grown at this temperature. In addition, the XPS data also indicate slightly decreased oxygen content in heavily doped films, which is consistent with the XRD results. A slight increase of the La/Sr ratio with increasing Ag repeat rate is also revealed, which can be understood as the result of atom collisions in the presence of Ag atoms during deposition. Some of the smaller strontium atoms may lose their dynamic energy by bumping into the larger Ag atoms and cannot reach the surface of the substrates.

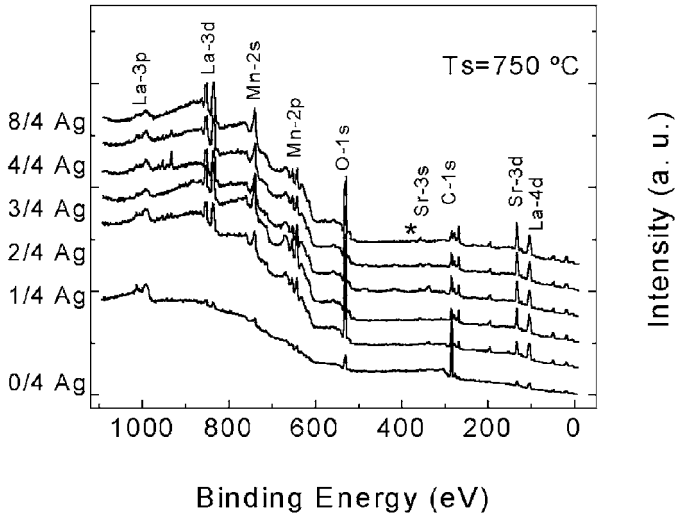

Figure 4. XPS spectrum for films deposited at 750 °C with different Ag repeat rates ranging from 1 to 8 Hz.

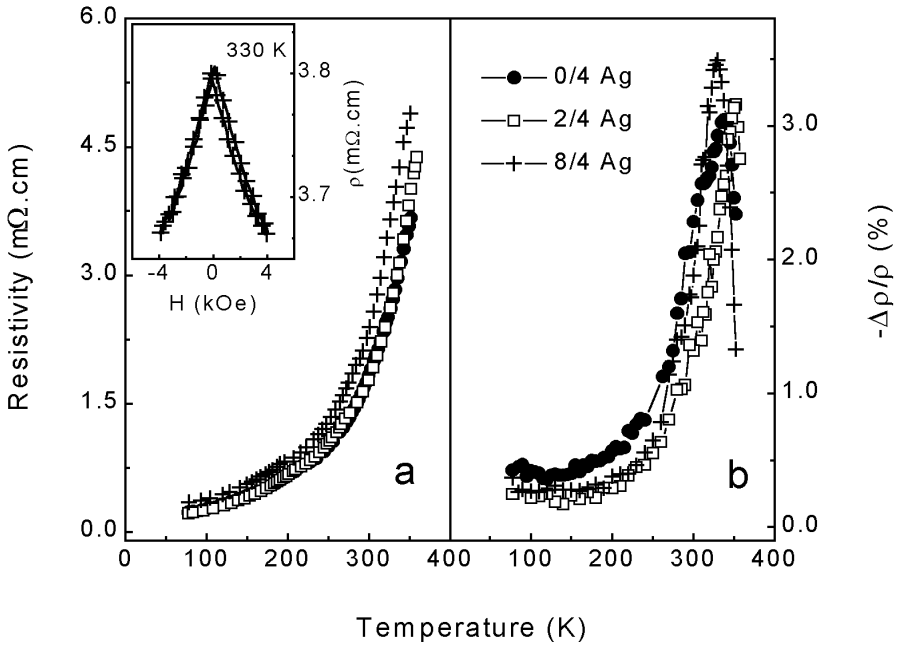

Figure 5. (a), (b) The $\rho(0)$–T curves, and the $\Delta\rho/\rho$–T curves measured in a field of 4 kOe for the films deposited at 750 °C with Ag repeat rates of 0 Hz, 2 Hz and 8 Hz, respectively. Inset is the $\Delta\rho/\rho$–H curve for sample $8/4\ Ag$ measured at T_{MR}.

The temperature dependency of $\rho(0)$ and magnetoresistance $\Delta\rho/\rho$(4 kOe) (defined as $(\rho(H) - \rho(H_c))/\rho(H_c)$) for the films co-deposited at 750 °C are shown in figures 5(a) and (b), respectively. Figure 5(a) indicates that all the films behave like a metal in the temperature range from 350 K to liquid nitrogen temperature (LN_2), thus the insulator–metal transition

temperatures T_{IM} are expected to be above 350 K. In LN_2, ρ of the stoichiometric LSMO film is only 0.23 mΩ cm, which indicates the high crystalline quality of the film. The ρ–T curves are almost superimposed on each other for sample *0/4* and *2/4 Ag*, while it is slightly higher for sample *8/4 Ag*. The $\Delta\rho/\rho$–T curves of the three films, as shown in figure 5(b), are also similar. $\Delta\rho/\rho$ shows a maximum of $\sim$3% in the vicinity of T_c, which is obviously lower than the T_{IM}, and declines with decreasing temperature. The negligible MR values in LN_2 imply that the low temperature eMR are suppressed, which indicates that the films deposited at 750 °C are high-quality epitaxial along the *c* axis and the GBs must be perfect small angles. The temperature corresponding to the $\Delta\rho/\rho$ maximum, T_{MR}, is slightly different for these films; they are 339, 351 and 330 K for sample *0/8*, *2/8* and *8/4 Ag*, respectively. Combined with the XRD and XPS results, the decrease in T_{MR}, as well as the slight enhancements in $\Delta\rho/\rho$ and ρ for the highly doped film *8/4 Ag* can be attributed to the oxygen deficiency. The similarities of ρ–T curves and $\Delta\rho/\rho$–T curves, for films deposited at varying Ag precipitation, demonstrate that Ag dopant cannot substitute into the LSMO lattice. Inset is the $\Delta\rho/\rho$–H curve for sample *8/4 Ag* measured at T_{MR}.

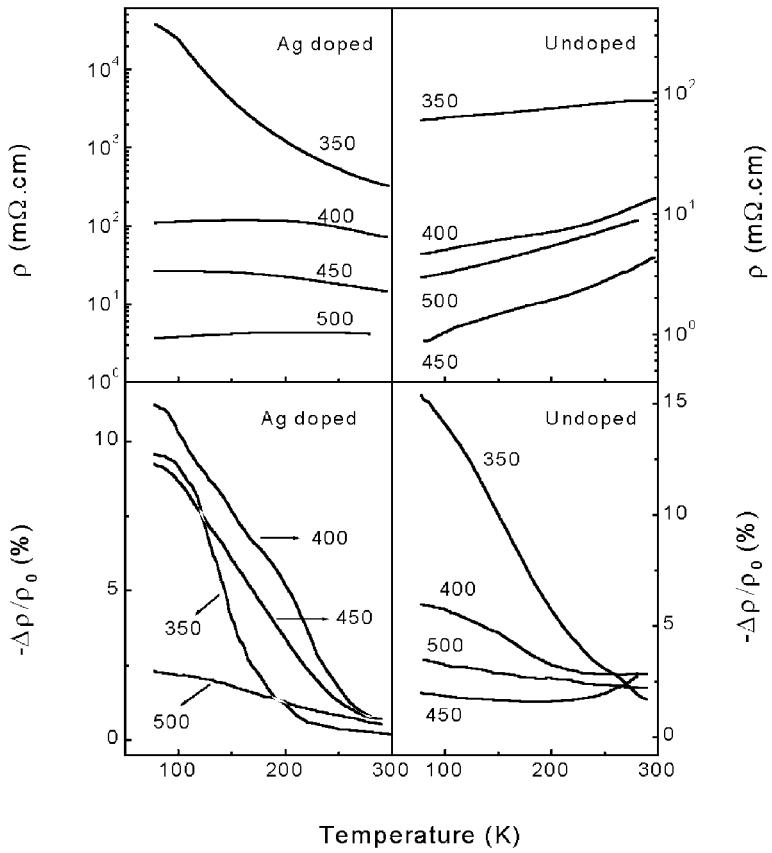

Figure 6. The temperature dependences of $\rho(0)$ and $\Delta\rho/\rho(4\ \text{kOe})$ for Ag-doped and undoped films deposited at T_s ranging from 550 to 350 °C, respectively.

3.3. Films deposited at reduced substrate temperatures

Ag-doped films deposited at purposely reduced substrate temperatures were also investigated. The temperature dependences of $\rho(0)$ and $\Delta\rho/\rho(4\,\mathrm{kOe})$ for films deposited at T_s ranging from 550 to 350 °C are shown in figure 6. Here the 'Ag-doped' refers to films deposited with Ag repeat rate of 8 Hz. All the undoped films deposited at different T_s behave like a metal from room temperature to 77 K, although ρ of the films deposited at lower T_s are higher due to the existence of amorphous phase among grains. Accordingly, $\Delta\rho/\rho$ of the undoped films increases fast with decreasing temperature, indicating the granular nature of the films. With declining T_s, the $\Delta\rho/\rho$ measured at LN_2 grows dramatically, from 2% at $T_s = 450\,^{\circ}\mathrm{C}$ to more than 15% at $T_s = 350\,^{\circ}\mathrm{C}$. It is noted that film deposited at 450 °C still shows a relatively large value of $\Delta\rho/\rho$ at room temperature, as a result of the summation of the intrinsic MR part. The somewhat abnormal behaviour shown by the film deposited at 500 °C is because of the co-existence of monoclinic and rhombohedral lattice structure in the films. 500 °C can be considered as a 'critical temperature' for growth of the two kinds of structure. Details will be reported later. However, different from the case of undoped films, the ρ–T curve for the Ag-doped films undergoes an insulator to metal transition at the temperature T_p ranging from room to 77 K. Moreover, ρ is about one order of magnitude higher than the undoped film deposited at the same T_s. The decrease of T_p can be considered as a consequence of the weakened inter-grain magnetic coupling by Ag doping. $\Delta\rho/\rho$–T curves of the Ag-doped films follow a similar trend as the undoped samples, except the greatly enhanced $\Delta\rho/\rho$ value at low temperature regions, especially in case of $T_s = 400$ and 450 °C. The $\Delta\rho/\rho$ value at 77 K for the Ag-doped film deposited at 400 °C is enhanced by a factor of two compared with the undoped, which is as large as 12% in a field of only 4 kOe. It is worth noting that ρ of the sample is only 10^2 mΩ cm. $\Delta\rho/\rho$ declines much slower with increasing temperature compared with the experimental data of insulator ($SrTiO_3$) doping [11]. At 200 K, $\Delta\rho/\rho$ of our sample is still larger than 5%, nearly 40% of the 77 K value, while the latter gives only less than 10%. As T_s is further reduced, the thickness of the amorphous phase among grains becomes larger; as a result, the sample behaves like an insulator during the whole temperature range. Accordingly, $\Delta\rho/\rho$ decreases much faster with increasing temperature. Therefore, different from the case of epitaxial thin films, Ag doping in granular films deposited at low T_s affects the film magneto-electrical properties significantly.

In order to reveal the origin of the enhanced eMR in the Ag-doped granular thin films, AFM was employed. Figures 7(a)–(d) and (f) show the morphology of films co-deposited at 400 °C with Ag repeat rates of 0, 1, 2, 4 and 8 Hz, respectively. Figure 7(e) is an AFM 'phase' image for the same scene as (b). The scale for each image is again $1 \times 1\ \mu\mathrm{m}^2$. Figure 7(a) is for the stoichiometric LSMO film deposited at 400 °C. Comparing with the undoped film deposited at 750 °C (figure 3(a)), it is clear that the grain shape becomes irregular and the grain size (GS) drops considerably with decreasing T_s. This suggests that the in-plane alignment is destroyed as T_s is reduced, although the *c*-axis texture still exists. With Ag doping, as shown in figure 7(b), the GS increase is negligible; instead, a kind of larger cluster is found scattering in the films. The phase scan shown in figure 7(e) indicates that the brightness of the clusters is different from that of the normal grains, which suggests different surface adhesion of the clusters and thus different physical properties of the two phases. The amount of the clusters increases with increasing Ag repeat rates, as shown in figures 7(c) and (d). As the Ag repeat rate is as high as 8 Hz (figure 7(f)), the clusters of size about 100–200 nm cover the entire visual field and result in apparently enlarged GS.

In order to investigate whether the larger clusters are due to Ag doping, TEM study of the sample *8/4 Ag* deposited at 400 °C (shown in figure 7(f)) was performed, and the result

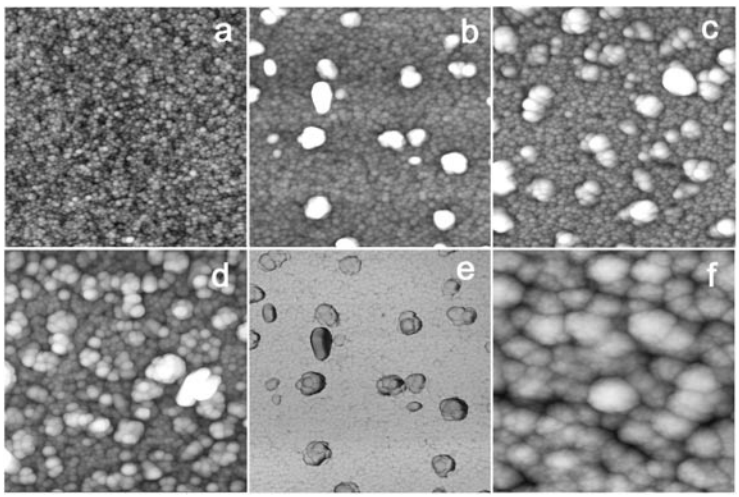

Figure 7. (a)–(d), (f) AFM images for the films co-deposited at 400 °C with Ag repeat rates of 0, 1, 2 and 8 Hz, respectively. (e) 'Phase' image for the same scene as (b). The scan areas for the images are all $1 \times 1\ \mu m^2$.

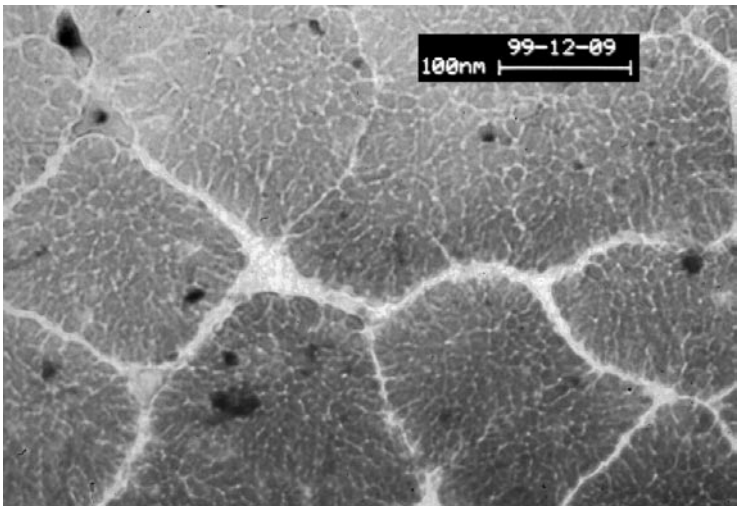

Figure 8. TEM image of the Ag-doped film shown in figure 7(f).

is shown in figure 8. It reveals that each 'cluster' consists of hundreds of sub-grains of size about 10–20 nm, similar to the GS of the undoped sample. An amorphous zone of about 10 nm wide exists between these clusters. Electron diffraction verified the polycrystalline/amorphous nature of the film. This image suggests that Ag dopant may act to 'glue' the sub-grains into larger clusters during the film deposition.

Meanwhile, the EDX spectrum, shown in figure 9, reveals the existence of Ag in the film. Investigation at points inside grains, at grain boundaries, and at some obviously inhomogeneous sites gave Ag content of about 5 at.%. The study shows no obvious segregation of Ag at the amorphous zone, which deviates from our instinctive expectation. We attribute this phenomenon to the selective sputtering during the TEM sample preparation. Considering the

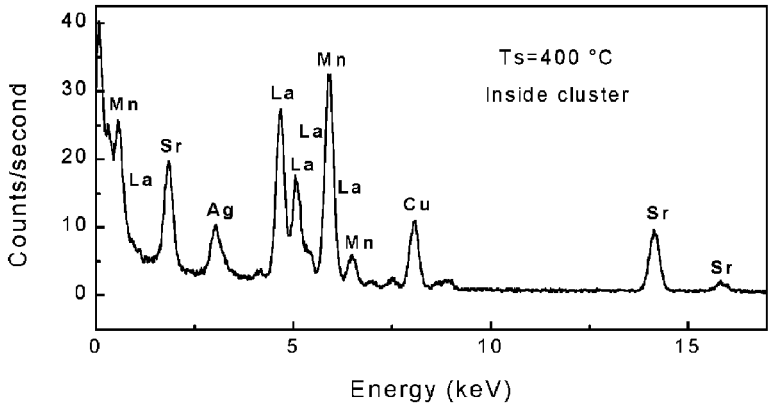

Figure 9. EDX spectrum measured at a point inside the 'clusters' for the Ag-doped film shown in figure 7(f).

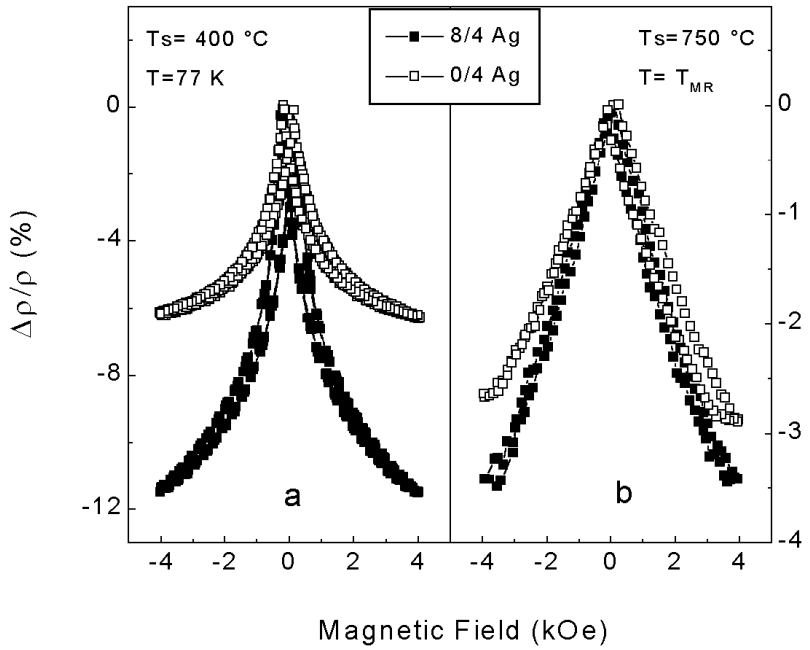

Figure 10. Comparison of the $\Delta\rho/\rho$–H loops measured for films deposited at 400 and 750 °C, respectively.

result of XRD, it is still reasonable to claim that, in the case of lower T_s, Ag exists at the amorphous zones among grains, and also the sub-grain boundaries. The Ag dopant serves as scattering centres and enhances the magnetic spin disorder at the boundaries, as a result enhancing the low temperature eMR value.

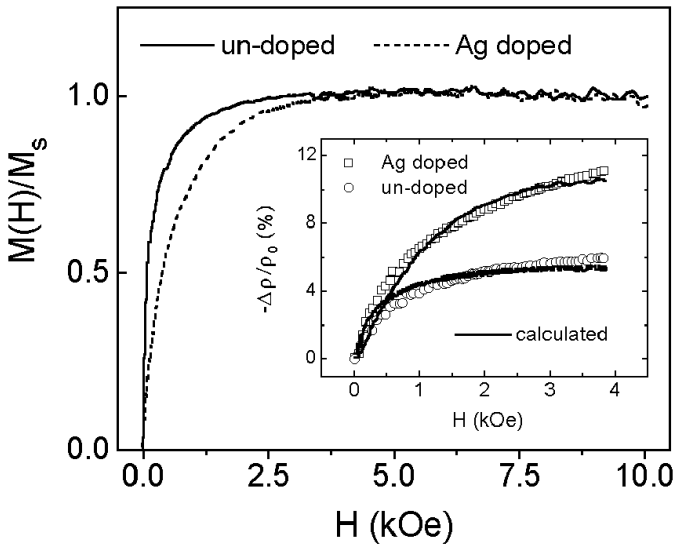

Figure 11. H dependence of M/M_s for Ag-doped and undoped films deposited at 400 °C. Inset are the experimental and calculated $\Delta\rho/\rho$ values as a function of H.

4. Discussions

In this experiment we expected to find out whether or not this Ag doping affects the manganese spin status at GBs, and enhances the eMR, as an insulator does. The findings reveal that it depends on the T_s during deposition.

The Ag-doping effects on the magnetoresistance in case of $T_s = 400\,^{\circ}\mathrm{C}$ and 750 °C are compared by figure 10. The right panel shows the magnetic field (H) dependence of the *intrinsic* MR, as revealed by the linear relationship, for the undoped and Ag-doped films deposited at 750 °C. The measurement is executed at the respective T_{MR} of the films. The figure indicates that, for the films deposited at this temperature, Ag has a slight effect on the magneto-electrical properties, most probably by causing oxygen deficiency. At $T_s = 750\,^{\circ}\mathrm{C}$, all the co-deposited films are *c*-axis epitaxial, as revealed by XRD results. Existence of Ag in the epitaxial thin films could not be detected. Based on the above investigations, a growth mechanism is established as follows: during deposition, the Ag dopant reaches to the surface of the substrate and diffuses to sites of lower free energy, such as the small angle grain boundaries. Meanwhile, the Ag atoms also serve as a 'catalyst' to enhance the inter-grain diffusion of the lattice species. As a result, defects in the GB regions are healed and the GB become blurred and fade in the case of higher doping concentrations. Finally, since the melting point of metallic Ag is only 962 °C [19], its saturated vapour pressure is fairly high at the deposition temperature, i.e., of the order of about 1×10^{-6} Torr [13] and the Ag atoms segregated in the GB regions will re-evaporate into the vacuum. Therefore, in the high T_s case, the increasing Ag precipitation only leads to gradual deterioration of the in-plane alignment, as shown by the AFM results, while it has little effect on the magneto-electrical properties of the thin films. It is also reasonable to assert that, in case of polycrystalline films, Ag doping will not affect the magneto-electrical properties *inside* grains.

The left panel shows the magnetic field (H) dependence of the *extrinsic* MR for the undoped and Ag-doped films deposited at 400 °C. The measurement is executed at 77 K. The figure indicates that Ag has considerable effect on the magneto-electrical properties of the films

deposited at this temperature, enhancing the MR value by a factor of two. Considering the discussion of the results of $T_s = 750\,^{\circ}$C, this enhancement can be attributed to the modification of the GBs by Ag doping. As $T_s = 400\,^{\circ}$C, the co-deposited films are granular with *c*-axis textures, as revealed by XRD and AFM results. Ag has been found at GBs and other defects. It 'glues' the *c*-axis oriented small LSMO grains together into clusters. Moreover, the Ag atom is of help in generating the amorphous phase among grains, and as a result increases the local Mn spin disorder at GBs. Therefore the low field eMR in the films is enhanced.

It is hard to determine the chemical status of the doped Ag atoms experimentally. However, according to the data of room temperature bond enthalpies [19], which gives Ag–Ag as ∼160 and Ag–O as ∼220 mJ mol^{-1}, it is reasonable to conclude that Ag tends to be oxidized in an oxygen ambient. However, since the bond enthalpy of O–O is about ∼498 mJ mol^{-1}, the LSMO lattice is more likely to obtain atomic 'O' by dissociation of Ag oxide than directly from O_2, and therefore the nearby LSMO grain acts as a reductive agent. The existence of metal Ag as an amorphous phase can be expected. As the impurity introduced in our sample is not a pure insulator, it does not increase the sample resistivity as much as CeO_2 or $SrTiO_3$.

Moreover, as we introduced before, the Ag-doping enhanced eMR declines much slower with increasing temperature than that enhanced by insulator doping. Figure 11 shows the normalized magnetization measured at 77 K of the two samples deposited at 400 °C, with and without Ag doping. The M/M_s–H curve of the undoped film is more 'square' than the Ag doped, indicating the pinning effect of Ag dopant on the alignment of the interface magnetic moments in a magnetic field. Both samples saturate at about 4 kOe, although H_s is slightly higher for the doped one. As shown in the inset, $\Delta\rho/\rho$ of the Ag-doped sample increases faster with magnetic field than the undoped one. The experimental eMR data of the two samples are fitted using the formula $\Delta\rho/\rho = \alpha(M/M_s)^2$, and the fitting results are also shown in the same inset. It is clear that the fitting is quite good, as long as the magnetic field is lower than 4 kOe. This may suggest that the transport mechanism underlying the Ag-doping enhanced eMR is spin-dependent scattering. Due to the constriction of our magnetic field, further analysis and the $\Delta\rho/\rho$–T curve fitting are difficult.

5. Conclusion

Providing it is doped by the method of dual-beam pulsed-laser ablation, Ag cannot substitute into the LSMO lattice, and thus will not affect the magneto-transport properties inside grains. Therefore the improvement of the inter-grain eMR in polycrystalline samples by Ag doping can be attributed to the enhancement of the magnetic spin disorders at GB regions. The metal Ag can also serve as strong scattering centres for the conducting electrons, as an insulator.

Acknowledgments

The author would like to thank Mr S L Lim for his work in the XPS measurement. Thanks are also due to Ms H Z Kong and Mr L Si for the assistance in the VSM experiment.

References

[1] Gupta A, Gong G Q, Xiao G, Duncombe P R, Lecoeur P, Trouilloud P, Wang Y Y, Dravid V P and Sun J Z 1996 *Phys. Rev.* B **54** 15 629
[2] Hwang H Y, Cheong S-W, Ong N P and Batlogg B 1996 *Phys. Rev. Lett.* **77** 2041
[3] Li X W, Gupta A, Xiao G and Gong G Q 1997 *Appl. Phys. Lett.* **71** 1124
[4] Lee S, Hwang H Y, Shraiman B I, Ratcliff W D II and Cheong S-W 1998 *Phys. Rev. Lett.* **82** 4508

[5] Coey J M D 1999 *J. Appl. Phys.* **85** 5576
[6] Steenbeck K, Eick T, Kirsch K, O'Donnell K and Steinbeiß E 1997 *Appl. Phys. Lett.* **71** 968
[7] Walter T, Dörr K, Müller K-H, Holzapfel B, Eckert D, Wolf M, Schläfer D and Schultz L 1999 *Appl. Phys. Lett.* **74** 2218
[8] Andrés A, García-Hernández M, Martínez J L and Prieto C 1999 *Appl. Phys. Lett.* **74** 3884
[9] Hueso L E and Rivas J, Rivadulla F and López-Quintela M A 1999 *J. Appl. Phys.* **86** 3881
[10] Balcells L I, Carrillo A E, Martinez B and Fontcuberta J 1999 *Appl. Phys. Lett.* **74** 4014
[11] Petrov D K, Krusin-Elbaum L, Sun J Z, Feild C and Duncombe P R 1999 *Appl. Phys. Lett.* **75** 995
[12] Liu J-M, Li J, Huang Q, You L P, Wang S J, Ong C K, Wu Z C and Liu Z G 2000 *Appl. Phys. Lett.* **76** 2286
[13] Moshfegh Z, Wang Y Q, Sun Y Y, Mesarwi A, Hor P H and Ignatiev A 1993 *Physica* C **218** 396
[14] Kalyanaraman R, Oktyabrsky S and Narayan J 1999 *J. Appl. Phys.* **85** 6636
[15] Shreekala R *et al* 1999 *Appl. Phys. Lett.* **74** 2857
[16] Tao T, Cao Q Q, Gu K M, Xu H Y, Zhang S Y and Du Y W 2000 *Appl. Phys. Lett.* **77** 723
[17] Ong C K, Xu S Y and Zhou W Z 1998 *Rev. Sci. Instrum.* **69** 1
[18] Li J, Liu J-M, Li H P, Fang H C and Ong C K 1999 *J. Magn. Magn. Mater.* **202** 285
[19] Kerr J A 1998 *CRC Handbook of Chemistry and Physics 1999–2000* 79th edn, ed D R Lide (Boca Raton, FL: Chemical Rubber Company)